A short note on the use of daily climate data to calculate Humidex heat-stress indices

Emilia Diaconescu, Housseyni Sankare, Kenneth Chow, Trevor Q. Murdock, & Alex J. Cannon

2023

Pacific Climate Impacts Consortium (PCIC)

PCIC Publications

Original citation:

Diaconescu, E., Sankare, H., Chow, K., Murdock, T. Q., & Cannon, A. J. (2023). A short note on the use of daily climate data to calculate Humidex heat-stress indices. International *Journal of Climatology*, *43*(2), 837–849. https://doi.org/10.1002/joc.7833

Received: 16 May 2022 | Revised: 29 July 2022 | Accepted: 12 August 2022 | Published on: 2 September 2022

DOI: 10.1002/joc.7833

RESEARCH ARTICLE

International Journal of Climatology RMetS

A short note on the use of daily climate data to calculate Humidex heat-stress indices

Emilia Diaconescu[1] | **Housseyni Sankare**[1] | **Kenneth Chow**[1] | **Trevor Q. Murdock**[1] | **Alex J. Cannon**[2]

[1]Canadian Center for Climate Services, Environment and Climate Change Canada, Gatineau, Québec, Canada

[2]Climate Research Division, Environment and Climate Change Canada, Victoria, British Columbia, Canada

Correspondence
Emilia Diaconescu, Canadian Center for Climate Services, Environment and Climate Change, Gatineau, QC, Canada.
Email: emilia.diaconescu@ec.gc.ca

Abstract

The projected increase in the frequency and intensity of extreme heat events due to climate change means an associated increase in risk of heat-related illnesses and mortality. Public health systems need to be prepared to identify and reduce the susceptibility of vulnerable populations to increased occurrence of heat-related illness and stress. To facilitate this, climate services have begun developing climate change projections for heat-stress indices based on exceedances of thresholds used operationally in meteorological heat warning systems. This task is complicated by the fact that heat-stress indices are generally computed using hourly data whereas climate model outputs are often archived at daily or longer time steps. This study focuses on Humidex, a heat-stress index used in heat alerts issued by the Meteorological Service of Canada. Several potential solutions for computing robust Humidex indices using daily data are examined, including a new approximation method. Indices obtained with the new method are compared with indices obtained using the classic method based on hourly data as well as with other two methods based on average daily values. The new approximation gives good estimations for humidex indices, while the daily-average-value methods present biases with respect to the hourly-value method.

KEYWORDS

climate change impacts, climate services, heat-stress indices, Humidex, relative humidity

1 | INTRODUCTION

Human health is directly influenced by several environmental conditions associated with temperature, humidity, wind, and incoming solar radiation. The term "heat stress" is often used to describe the heat-related impacts on human health that are associated with high values of air temperature, humidity, and solar and thermal radiation (Schwingshackl *et al.*, 2021). Exposure to extreme heat-stress can lead not only to loss of work productivity (Dunne *et al.*, 2013; Kjellstrom *et al.*, 2013) but also to dehydration, heat stroke, and many cardiovascular, respiratory, and cerebrovascular diseases, depending on the time of exposure and intensity of stress (McMichael and Lindgren, 2011; Mora *et al.*, 2017).

Many meteorological services around the globe have developed operational systems to alert the public of the danger of heat stress (Schwingshackl *et al*., 2021). An alert is usually issued when an index related to heat-stress is forecast to be greater than a specific threshold value. Examples of heat-stress indices include Environment and Climate Change Canada (ECCC) Humidex (Masterton and Richardson, 1979), NOAA heat index (Steadman, 1979; Rothfusz, 1990), Australian Bureau of Meteorology Simplified Wet-Bulb Globe Temperature (Buzan *et al*., 2015), and Perceived Temperature (Staiger *et al*., 2012). The Wet-Bulb Globe Temperature is often used for heat safety recommendations for athletes and worker productivity (Chavaillaz *et al*., 2019). Schwingshackl *et al*. (2021) summarizes the definitions of many heat-stress indices and presents a table with the exceedance thresholds used for each of them.

Humidex (HX) is a relatively simple index, depending only on temperature and relative humidity, and is easier to calculate compared to other more complex indices (e.g., the Universal Thermal Climate Index, the Wet-Bulb Globe Temperature). For these reasons, HX has been adopted in other parts of the world (see, e.g., Golbabaei *et al*., 2021 for Iran; Scoccimarro *et al*., 2017 for Europe; Středová *et al*., 2015 for Czech Republic; Giannopoulou *et al*., 2014 for Greece; Alfano *et al*., 2010; Infusino *et al*., 2021 for Italy). In Canada, meteorological forecasts are usually accompanied by recommendations based on threshold values of HX. For example, it is recommended that outdoor activities be moderated depending on age and health conditions when the HX exceeds 30, and that all unnecessary outdoor activities cease completely when it reaches 40 (Mekis *et al*., 2015).

The average temperature has shown a warming trend in recent decades over the entire world (IPCC, 2013). Global surface temperature over land was 1.59°C warmer in 2011–2020 than in 1850–1900 (IPCC, 2021). In Canada, the linear trend indicates an increase of 1.7°C in mean temperature over the 1948–2016 period, with six (6) of the 10 warmest years during the last 15 years (Bush and Lemmen, 2019). There is also a steady increase in the number of countries that have reported new maximum temperature records (Martínez-Austria and Bandala, 2018) and in the number of regional heat waves (Perkins-Kirkpatrick and Lewis, 2020). Some of them are occurring in regions not accustomed to facing hot conditions. For example, Siberia reported a heat wave with extreme monthly temperatures of +6°C anomalies from January through May 2020 (Overland and Wang, 2021). Another example is the June–July 2021 U.S. Pacific Northwest and Western Canadian heat wave that took communities by surprise with the hottest temperature of 49.5°C ever recorded in Canada and anomalies of maximum temperatures for the time of year of +16 to +20°C (Philip *et al*., 2021).

Climate models project an increase in the mean temperature as well as in the probability of extremes, including heat wave events (IPCC, 2013; IPCC, 2021). The Intergovernmental Panel on Climate Change (IPCC) sixth assessment report (IPCC, 2021) shows that global temperature is projected to reach the 2°C warmer the pre-industrial levels in the 2040s in the case of the high-carbon pathway (the SSP5-8.5 scenario). The projected warming is greater at high latitudes where the population is not prepared to deal with long and frequent periods of hot temperatures. For example, the mean temperature in Canada is projected to increase at 1.92 (1.90–1.94) times and 1.98 (1.96–2.01) times the global rate according to projections from large (>20 members) CMIP5 and CMIP6 ensembles, respectively (Sobie *et al*., 2021). This means that at 2°C of annual mean global surface air temperature increase, Canada is projected to warm by 3.9°C (2.7–4.7°C) in CMIP5 and by 4.1°C (3.1–4.9°C) in CMIP6 (Sobie *et al*., 2021).

The warming associated with climate change constitutes a serious threat to future living and working environments and human health. The severity of those risks will depend on the ability of public health and safety systems to address these changing threats (McMichael and Lindgren, 2011). Developing climate change projections for heat-stress indices used in meteorological alerts, and for the exceedances of thresholds already established in heat warning systems and occupational health, will help with preparedness efforts of public health and safety systems for adaptation to climate change. For HX, indices like the annual number of days with HX greater then 30, 35, or 40 can be very useful. Mekis *et al*. (2015) analysed trends in historical values (1953–2012) of those HX-based indices across Canada using hourly observations at 126 stations. The indices have statistically significant positive trends at many stations and for most of the large urban centres. However, producing projections of those indices is not an easy task because they are based on hourly values, whereas outputs from climate models are frequently only available on a daily time step. The same issue stands for the other heat-stress indices and threshold exceedance products.

First, this study demonstrates that standard methods that rely on daily mean temperature and humidity data to calculate HX and exceedance of HX thresholds produce daily indices that differ from those computed directly from hourly values. Second, this study proposes a new approach that enables the reliable estimate of daily HX indices using daily temperature and humidity data.

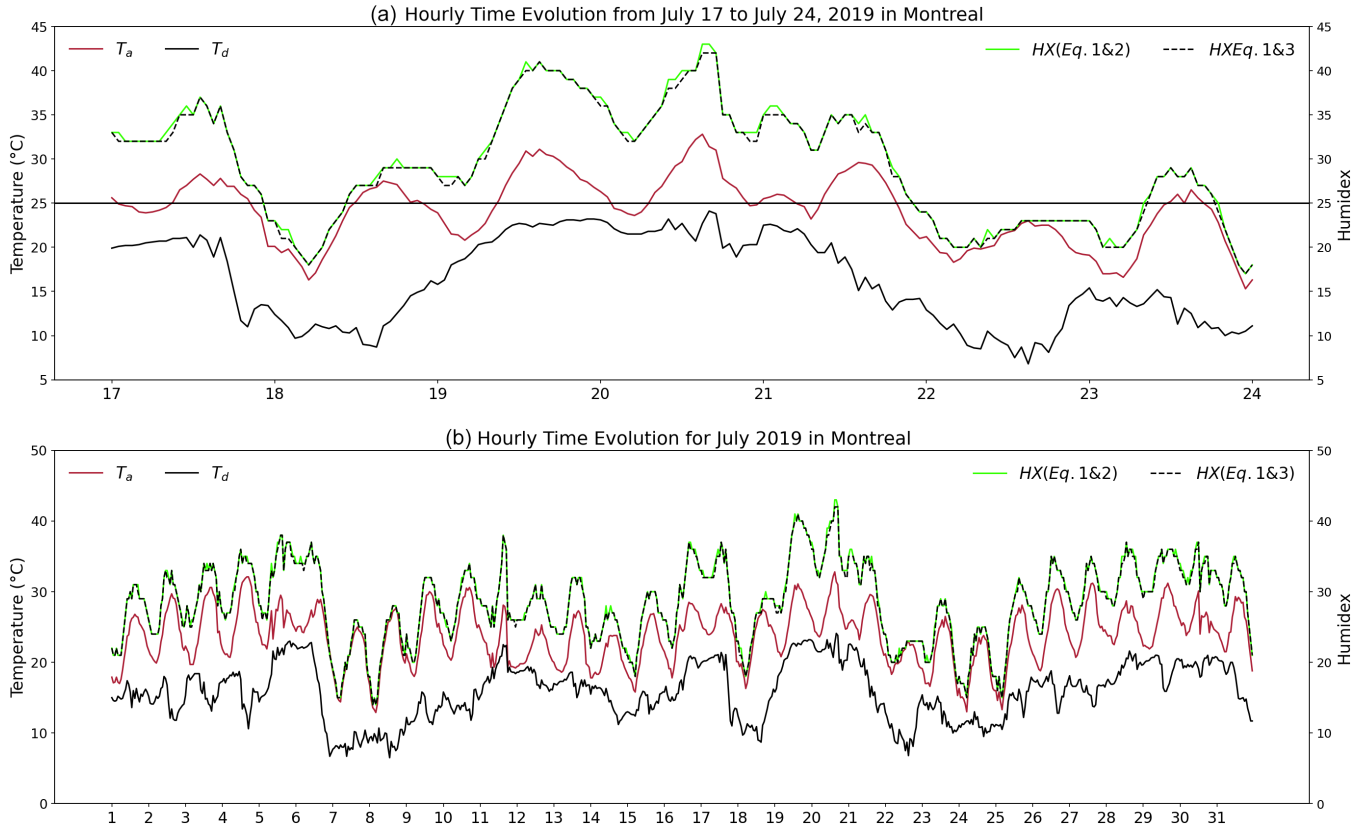

FIGURE 1 Time evolution for HX computed with ρ from Equation (2) and from Equation (3), T_a, and T_d over a short period of 1 week (a) and a month (b) in July 2019 at the Montréal-Pierre Elliott Trudeau International Airport. The horizontal line in (a) denotes the threshold that determines when HX is included in forecasts for the station [Colour figure can be viewed at wileyonlinelibrary.com]

2 | DATA AND METHODS

2.1 | Humidex definition and characteristics

HX is an empirical heat-stress index introduced by Masterton and Richardson (1979) that relates outdoor thermal discomfort experienced by the general population with air temperature and humidity. HX is expressed as a linear combination of air temperature T_a (°C) and the vapour pressure of water ρ (hPa),

$$\mathrm{HX} = T_a + \frac{5}{9}(\rho - 10), \tag{1}$$

$$\rho = 6.11 \times \mathrm{e}^{5417.7530\left(\frac{1}{237.16} - \frac{1}{T_d}\right)}, \tag{2}$$

where T_d is dew point temperature (K). However, outputs of ρ and T_d are usually not archived from climate models. Instead, approximations are used to express ρ using relative humidity RH (%) or specific humidity q and surface air pressure Ps (Pa),

$$\rho = 6.112 \times 10^{7.5 \times T_a/(237.7+T_a)} \times \mathrm{RH}/100, \tag{3}$$

$$\rho = \frac{q \times P_s}{0.622 + q}. \tag{4}$$

Figure 1 presents an example of the time evolution for HX (with ρ computed from Equations (2) and (3)), T_a and T_d over a period of 1 week (Figure 1a) and 1 month (Figure 1b) using hourly data from a meteorological station at Montreal, Canada. There is a great similarity between the two estimations and HX is generally correlated with T_a.

HX is typically computed hourly, with values included in the 24-hr forecast when HX $\geq$ 25, $T_d > 0$°C, and $T_a \geq 20$°C. Table 1 presents the degree of discomfort associated with different thresholds and ranges of HX values and describes the associated response plan of Occupational Health Clinics for Ontario Workers (Alfano *et al.*, 2010).

As T_a increases due to climate change, an increase in the number of days per year with HX greater than those thresholds is expected. Hence, these thresholds can also be used to develop climate indices with impact-

TABLE 1 Ranges of the HX index suggested by the humidex heat stress response plan by occupational health clinics for Ontario workers

Humidex range	Thermal discomfort level	Response
25°C ≤ HX ≤ 29°C	Discomfort perceived by a few people	Supply water to workers on an "as needed" basis
30°C ≤ HX ≤ 33°C	Noticeable discomfort	Post heat stress alert notice Encourage workers to drink extra water Start recording hourly T_a and RH
34°C ≤ HX ≤ 37°C	Evident discomfort	Start recording hourly T_a and RH Post heat stress warning notice Notify workers that they are drinking extra water Ensure workers are trained to recognize symptoms
38°C ≤ HX ≤ 39°C		Provide 15 min relief per hour Provide adequate cool (10–15°C) water Provide at least 1 cup (240 mL) of water every 20 min Workers with symptoms should seek medical attention
40°C ≤ HX ≤ 42°C	Intense discomfort. Avoid efforts	Provide 30 min relief per hour in addition to the provisions listed previously
43°C ≤ HX ≤ 44°C		If feasible provide 45 min relief per hour in addition to the provisions listed above If a 75% relief period is not feasible then stop work until the HX is 42°C or less
45°C and over	Serious danger. Suspend physical activities	Stop work until the HX is 44°C or less

relevant thresholds (Mekis *et al.*, 2015; Schwingshackl *et al.*, 2021).

2.2 | Proposed approximation

Mekis *et al.* (2015) has used three threshold exceedance indices based on daytime hourly HX for Canada. They are defined as the annual number of days with one or more hourly HX value >30, 35, or 40. Our objective is to obtain the same indices using daily data instead of hourly data. The proposed methodology is based on the fact that "the count of the number of annual days with at least one hourly HX value greater than a specific threshold" is equivalent to counting the number of annual days with "daily maximum HX (HXmax)" (computed from hourly data) greater than that threshold. Therefore, calculation of the indices can be done if a robust approximation of daily HXmax can be obtained that does not directly require hourly HX records.

Figure 1 shows that daily HXmax generally occurs at the time of daily maximum T_a (Tmax). This observation is confirmed by the climatological diurnal cycle of T_a and HX shown in Figure 2 and suggests that daily HXmax can be approximated using:

- Daily Tmax and RH at the time of Tmax via Equations (1) and (3), or
- Daily Tmax, q at the time of Tmax, and Ps at the time of Tmax via Equations (1) and (4).

Generally, archived climate model outputs only include daily mean q or RH and daily Tmax, or, more recently, daily minimum RH (RHmin).

Some previous studies have used daily HX and threshold indices obtained using daily mean q and Ps instead of q and Ps at the time of Tmax. For example, Zhao *et al.* (2015) and Mistry (2020) used daily means of T_a, q, and Ps; Schwingshackl *et al.* (2021) used daily Tmax and daily mean q and Ps. It is important to note that T_d, q, and Ps do also vary during the day but they do not have a clear diurnal cycle. This is evident in Figure 1 for T_d. Consequently, it is difficult to find relationships between daily HXmax and daily values of T_d, or q and Ps at the time of Tmax that are valid for climatological studies.

Figure 2 compares the diurnal cycles of T_a and HX cycles to that of RH computed from hourly measurements at Montréal-Pierre Elliott Trudeau International Airport. At the time of Tmax (when HX is also at its maximum), RH is at its minimum. Therefore, using daily mean RH with daily Tmax will result in an overestimation of daily HXmax. However, combining daily Tmax with daily RHmin could result in a good approximation of daily HXmax and thus threshold exceedance indices.

Here, we propose approximating daily HXmax using daily Tmax and daily RHmin in Equations (1) and (3)

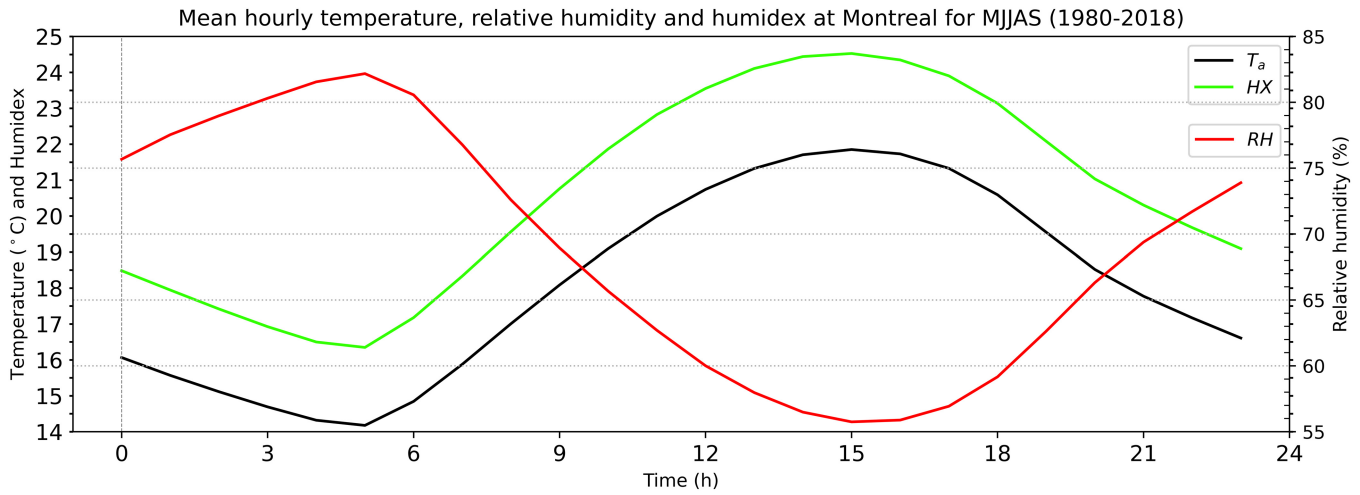

FIGURE 2 Average summer (May–September) 1980–2018 diurnal cycles of 2 m T_a, RH, and HX measured at Montréal-Pierre Elliott Trudeau International Airport. T_a and HX reach the daily maximum at 16 h00, when RH is at the daily minimum [Colour figure can be viewed at wileyonlinelibrary.com]

and next computing the annual number of days with daily HXmax > 30, 35, or 40 (HXmax30, HXmax35 and HXmax40, respectively).

2.3 | Data and evaluation methods

To validate the approximation, we used hourly T_a and RH data for the 1980–2018 period from the National Climate Archive of Environment and Climate Change Canada (ECCC). As HX is an outdoor index and the exceedances of HX thresholds of interest in Canada only occur in the warmer months of the year, the analysis is restricted to local standard times between 0700 and 1900 LST (UTC-4 for Atlantic regions to UTC-7 for British Columbia) in the months of May to September. Approximately 2000 stations in the ECCC archive have hourly data. Completeness criteria were used to select stations with sufficient length for climate analysis: stations that were retained have no more than 20% missing data and at least 15 valid years during the 1980–2018 period.

A total of 319 stations meet these criteria (Figure 3). There are at least 100 stations valid for each year over the 1980–2018 period. The stations are fairly well distributed across Canada, with a greater number of stations situated in southern Canada, which is the region where HX can exceed the impact thresholds listed in Table 1. The northern half of Canada is characterized by a cold climate and the impact thresholds there are rarely exceeded.

Only days with fewer than 3 hr of missing data (during the 0700 to 1900 LST) were used in subsequent calculations.

The evaluation of the approximation was done in two steps:

1. Daily HXmax approximation from daily Tmax and daily RHmin were compared with daily HXmax obtained directly from hourly HX and other daily value approximations.
2. HXmax30, HXmax35, and HXmax40 indices obtained using daily HXmax approximation were compared with those obtained from hourly HX.

The datasets are computed as follows.

Hourly records for T_a and RH from the selected stations were used to compute hourly HX using Equations (1) and (3); hourly HX values are next used to compute the control dataset for daily HXmax (noted HXmax-HR) against which the approximated daily HXmax will be validated. The proposed approximation (noted as A1) is replacing T_a and RH in Equations (1) and (3) with daily Tmax and daily RHmin. Because daily RHmin is not archived for all climate models, but most of them have daily RHmean, two other approximations (noted as A2 and A3) were computed for comparison. They are obtained by replacing T_a and RH in Equations (1) and (3) with daily Tmean/Tmax and daily RHmean. Table 2 summarizes all datasets with daily HXmax and their notations.

The skill of each approximation in estimating the annual indices and the daily HXmax was determined using three metrics: the Perkins' skill score (which measures the overlap of distributions of daily values), the mean bias, and the root mean square error (RMSE). Values of these three statistical metrics are presented at every station on maps in section 3.

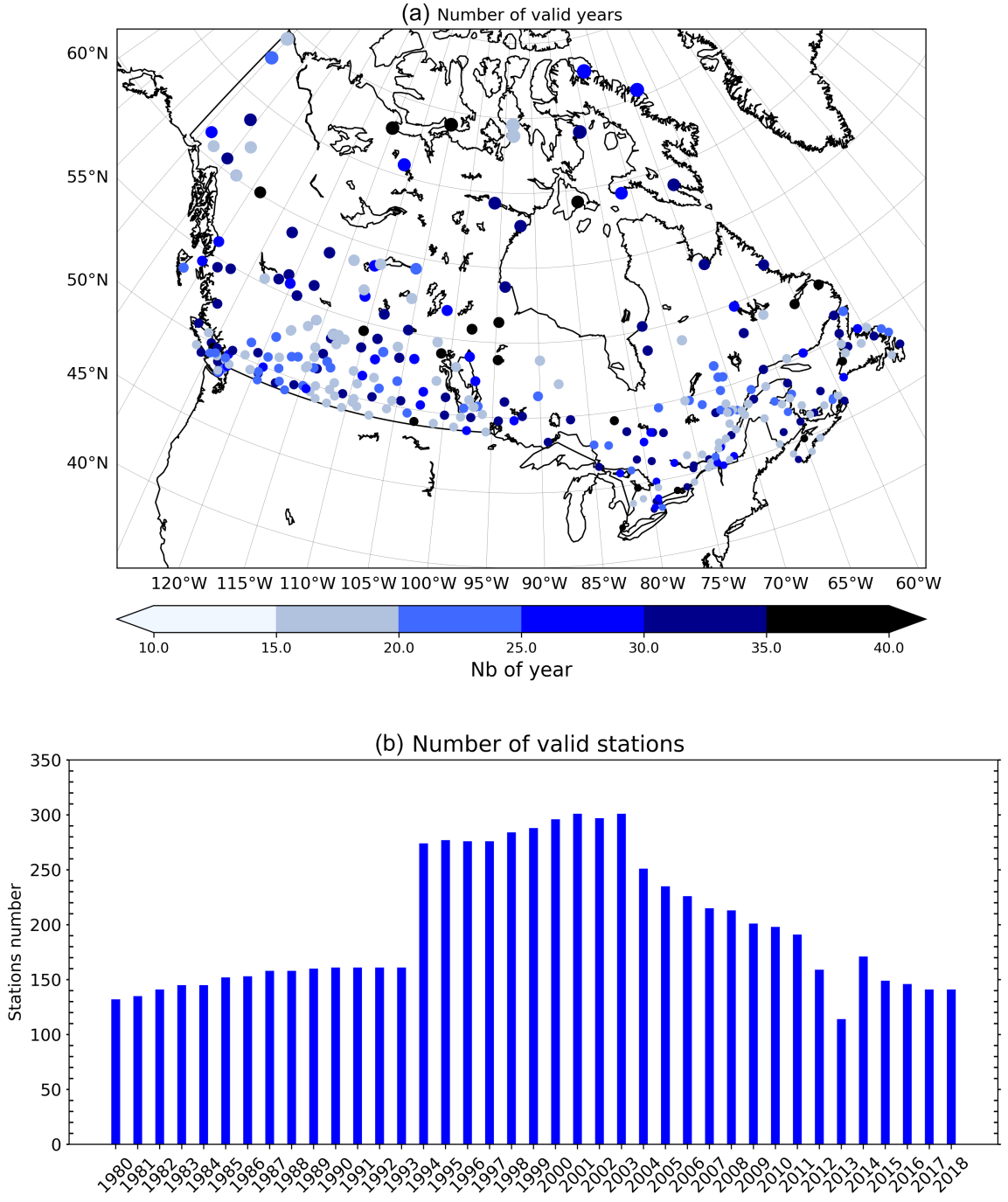

FIGURE 3 Spatial (a) and temporal (b) distribution of stations that meet selection criteria. The colours in (a) indicate the number of valid years per station, and the bars in (b) indicate the number of stations that meet the criteria for each year. A valid year is a year with less than 20% missing data for the months of May to September, from 0700 to 1900 LST [Colour figure can be viewed at wileyonlinelibrary.com]

The Perkins' skill score (PSS) is a robust metric that has been used in many studies to evaluate temperature and precipitation distributions (e.g., Perkins *et al.*, 2007; 2009; 2012; Maxino *et al.*, 2008; Pitman and Perkins, 2009; Boberg *et al.*, 2010; Kjellstrom *et al.*, 2010; Kabela and Carbone, 2015; Diaconescu *et al.*, 2018). It is defined as the overlap between two empirical probability density functions (EPDF) and has the advantage of being independent of the shape of the underlying distribution, thus applicable to any variable. In this study, normalized histograms of daily HXmax values from the three approximations were compared with corresponding histograms of daily HXmax from the control dataset, for each station, with a bin size of 1 unit. The metric was computed as the common area between the two distributions using the formula:

TABLE 2 Approximations used for HXmax

Daily HXmax dataset notation	Description
HXmax-HR	Hourly HX is computed using Equations (1) and (3), and daily HXmax is obtained as daily maximum of hourly values
HXmax-A1	Daily HXmax is obtained by replacing T_a and RH in Equations (1) and (3) with daily Tmax and daily RHmin
HXmax-A2	Daily HXmax is obtained by replacing T_a and RH in Equations (1) and (3) with daily Tmean and daily RHmean
HXmax-A3	Daily HXmax is obtained by replacing T_a and RH in Equations (1) and (3) with daily Tmax and daily RHmean

$$\mathrm{PSS}_k = \sum_{x=1}^{n} \mathrm{minimum}(\mathrm{EPDF}_k(x), \mathrm{EPDF}_O(x)), \quad (5)$$

where n is the number of bins used to calculate the normalized histograms, EPDF_k (x) is the frequency in bin x for the dataset k, $\mathrm{EPDF}_O(x)$ is the corresponding frequency for the recorded dataset in bin x. PSS values range from zero to one, a zero value corresponding to no overlap between the two distributions and one to identical distributions.

Scatter plots with regression lines and correlation coefficients for daily HXmax and time evolutions of indices are presented for two stations, which were selected as representative examples for most stations.

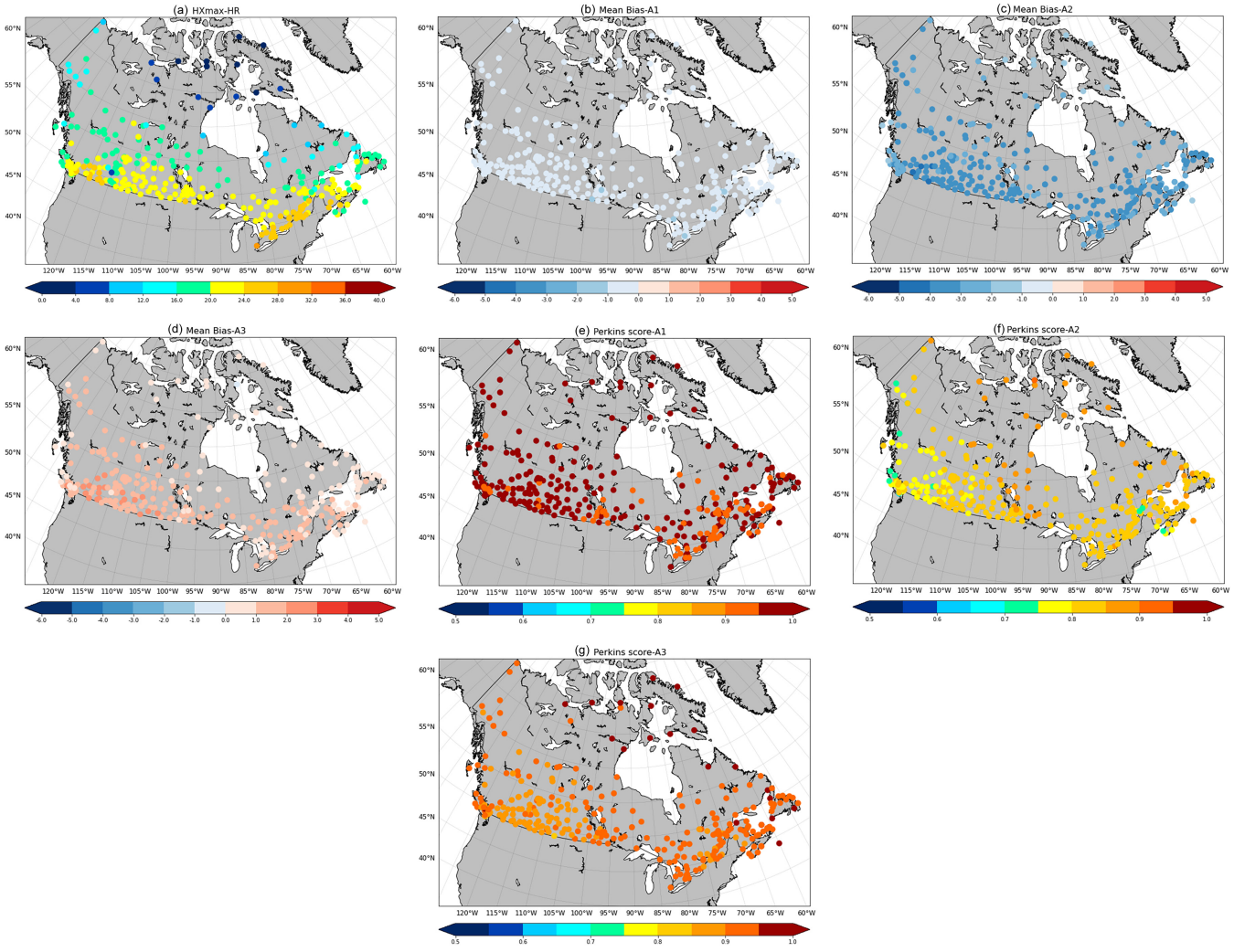

FIGURE 4 May–September (1980–2018) daily HXmax statistics for 319 stations across Canada, showing (a) the climatological mean for the control method, (b) mean bias for approximation A1, (c) mean bias for approximation A2, (d) mean bias for approximation A3, (e) Perkins skill score for approximation A1, (f) Perkins skill score for approximation A2, and (g) Perkins skill score for approximation A3 [Colour figure can be viewed at wileyonlinelibrary.com]

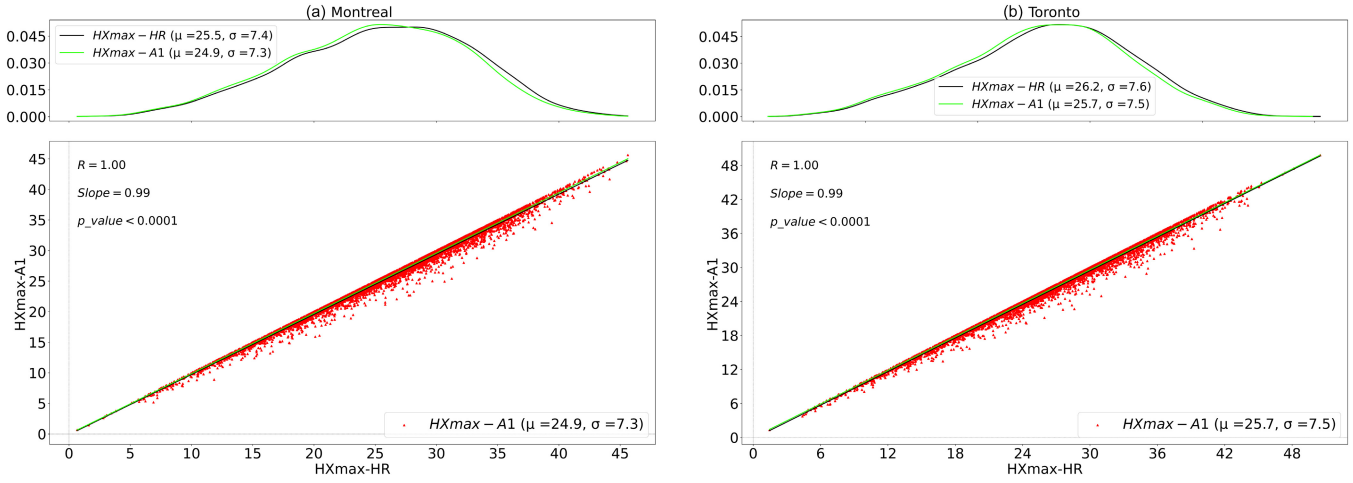

FIGURE 5 Frequency distributions (top panels) and scatterplots (bottom panels) of control and A1-approximated HXmax at (a) Montreal and (b) Toronto. Scatterplots show daily HXmax-A1 on the vertical axis and daily HXmax-HR (control dataset) on the horizontal axis. The correlation coefficient, the slope and *p*-value are indicated on the scatter plots. The mean (μ) and standard deviation (σ) for each distribution are indicated in the legend [Colour figure can be viewed at wileyonlinelibrary.com]

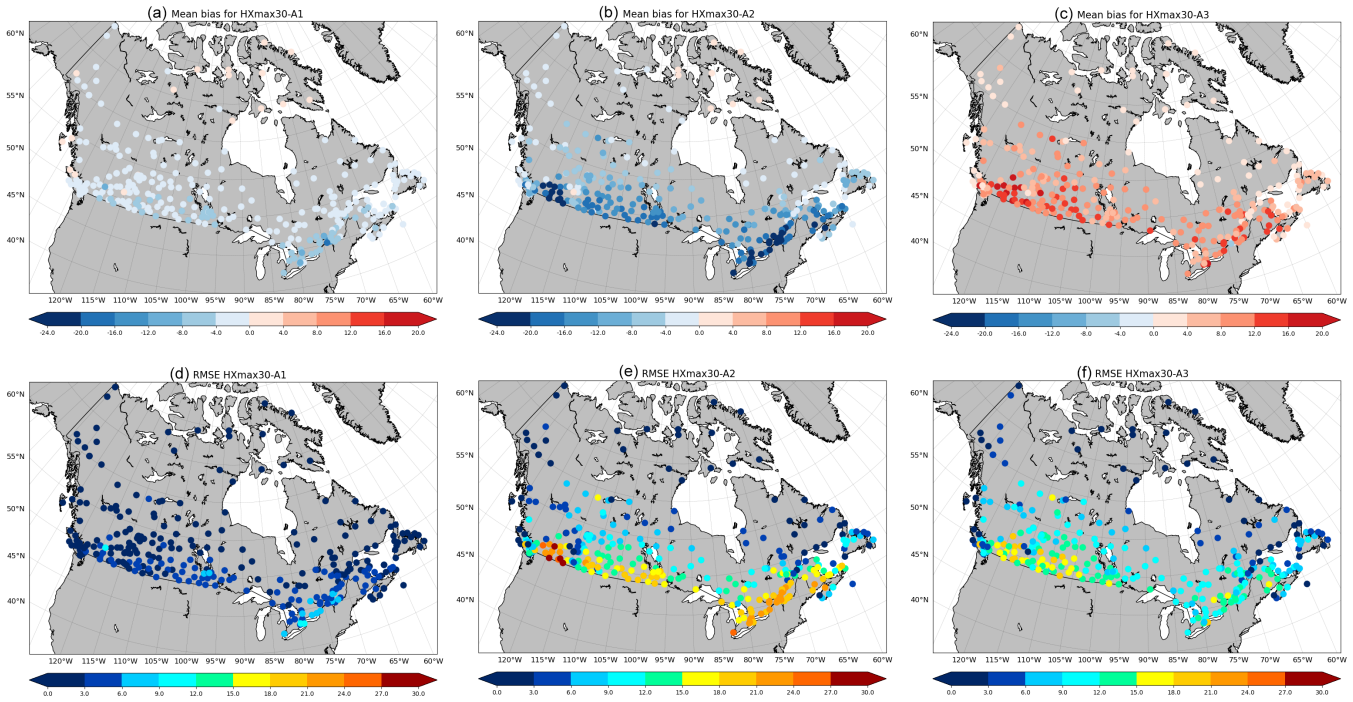

FIGURE 6 Mean bias and RMSE for the approximations (a, d) A1, (b, e) A2, and (c, f) A3, for HXmax30, and for 319 stations across Canada [Colour figure can be viewed at wileyonlinelibrary.com]

3 | RESULTS

3.1 | Daily HXmax evaluation

Figure 4 shows long-term mean values over the 1980–2018 period for the daily HXmax obtained with the control method, as well as the mean bias and the Perkins skill score for the daily HXmax estimated with the three approximations.

As expected from the diurnal cycle presented in Figure 2, approximation A3, using daily Tmax and daily RHmean leads to overestimation of HXmax at all stations (the mean bias in Figure 4d varies between −0.2 and +2.5). Approximation A2 (i.e., daily Tmean and daily

RHmean) provides an estimate of daily HXmean, which subsequently results in an underestimate of daily HXmax (the mean bias in Figure 4c varies between −4.4 and −1.5). Approximation A1 produces HXmax estimates that are more similar to the control dataset, with small negative mean biases between −1.3 and 0.0, and an average bias of 0.5 (Figure 4a). Perkins skill scores show that the distributions of daily HXmax obtained from approximation A1 are very close to those from the control method (values of Perkins score in Figure 4e are between 0.91 and 0.98 with an average value of 0.96, showing that at least 91% of distributions are overlapping at every station). Perkins scores are smaller for approximation A2 (between 0.61 and 0.90) and approximation A3 (between 0.84 and 0.97).

For each station, we have also computed the correlation coefficient between daily values from the control dataset and the approximation A1, which are close to 1 for all stations.

Figure 5 presents frequency distributions and scatterplots of daily values obtained for two locations with high HX values and typical mean bias (Montreal and Toronto) to illustrate the strength of the correlation, the typical magnitude of the negative bias, and the similarity of distributions for approximation A1. For both locations, approximation A1 and the control method have the same standard deviation and they overlap at 96%. The small difference is due to a shift in the mean of the distribution of approximation A1 toward smaller values. The small negative bias is also visible in the scatter plot despite a high correlation coefficient. Similar results are obtained at all stations.

The analysis of the correlation coefficients, the mean bias and the Perkins scores shows that the use of daily HRmin and Tmax in Equations (1) and (3) (approximation A1) works very well for daily HXmax. The errors are greater for the approximations A2 and A3. However, approximation A3 performs better than approximation A2 because the errors in A2 arise from poor estimation of the RH (replacing RH at the time of HXmax with

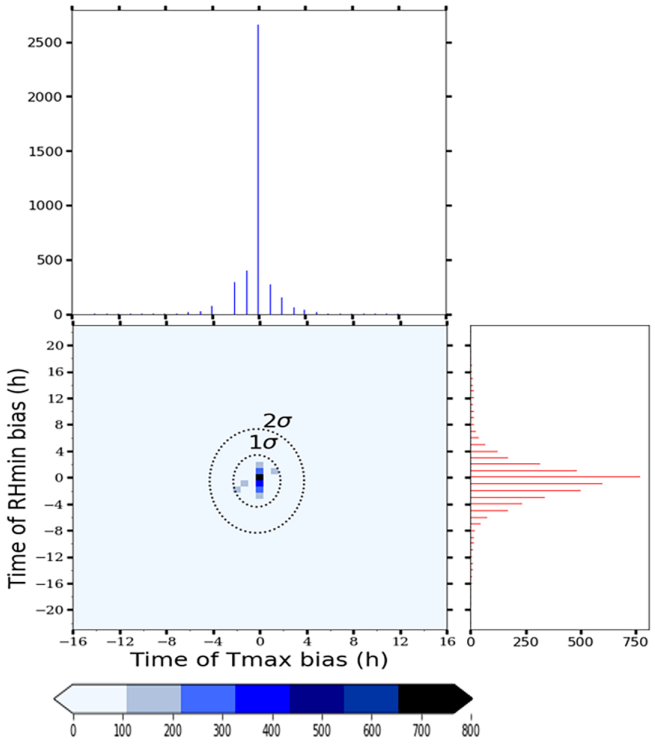

FIGURE 7 Bivariate (central figure) and univariate (lateral figures) histograms of the bias between the time of occurrence of daily Tmax and daily HXmax and the time of occurrence of daily RHmin and daily HXmax, for Toronto [Colour figure can be viewed at wileyonlinelibrary.com]

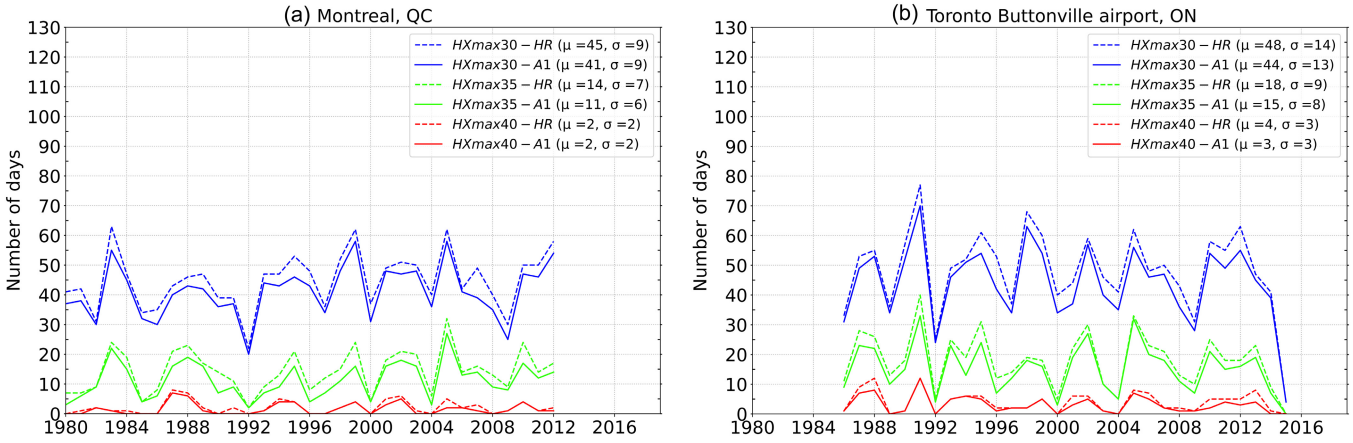

FIGURE 8 Time evolution of three HX indices (HXmax30, HXmax35 and HXmax40). The dashed lines show indices computed using the control method (with hourly HX) and the solid lines show indices computed using daily HXmax approximation A1 (with daily Tmax and daily RHmin). The mean (μ) and standard deviation (σ) for each dataset are indicated in the legend [Colour figure can be viewed at wileyonlinelibrary.com]

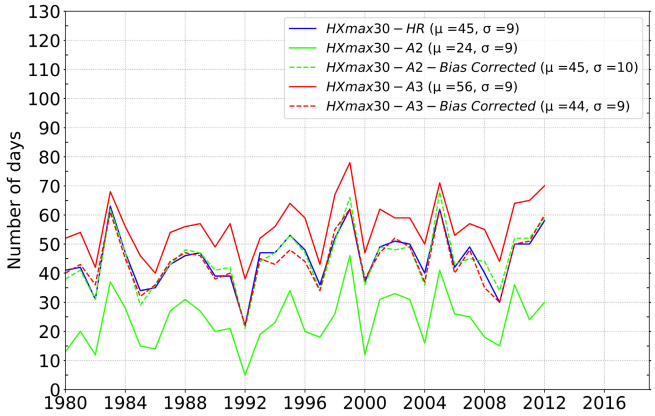

FIGURE 9 Time evolution of HXmax30 at Montreal for hourly HX, approximation A2, and approximation A3 with the bias corrected versions presented with dash lines. The mean (μ) and standard deviation (σ) for each dataset are indicated in the legend [Colour figure can be viewed at wileyonlinelibrary.com]

RHmean), while A3 also includes errors due to poor estimation of temperature (using Tmean instead of Tmax in the estimation of the HXmax).

3.2 | HXmax30, HXmax35, and HXmax40 evaluation

HXmax30, HXmax35, and HXmax40 indices obtained from the three daily approximations described in the previous section were compared with the equivalent control indices obtained from hourly data. As an example, Figure 6 shows the mean bias and the RMSE of HXmax30 over the 1980–2018 period.

Approximation A1 has the smallest RMSE and smallest mean biases. As for the daily HXmax, approximation A2 has larger errors than approximation A3. The average RMSE for approximation A1 is 3 days (Figure 6d) compared to 11 days and 10 days for approximations A2 and A3, respectively (Figure 6e,f). Approximation A3 leads to overestimates of threshold exceedances: the average mean bias is 8 days (Figure 6c), whereas approximation A2, based on daily HXmean, leads to substantial underestimates at most stations: the average mean bias is −10 days (Figure 6b) and there are locations where the mean bias exceeds −20 days. Approximation A1 provides the most accurate estimates; stations typically have biases less than 2.5 days (Figure 6a). These small biases are due to the fact that the times of occurrence of daily HXmax, daily Tmax, and daily RHmin are not always identical. This is evident in the example presented in Figure 7, which plots the differences in the times of occurrence of daily Tmax/RHmin with respect to daily HXmin as histograms, for Toronto.

The times of occurrence of daily Tmax and daily HXmax coincide for most of the days (most of the days are located in the central bin centred on 0). However, this occurs less often for daily RHmin, which has a broader distribution of differences, with most of the values situated between 4 and −4 hr. The fact that the HXmax30 obtained with approximation A1 only has small biases despite this temporal variation in RHmin is due to the fact that Tmax has a larger influence on HXmax than RHmin.

Similar conclusions are obtained for HXmax35 and HXmax40, although the biases are smaller because there are fewer days per year at these levels. As an example, Figure 8 compares the time evolution of the three indices calculated using approximation A1 against the hourly control indices at Montreal and Toronto (these cities have mean biases and RMSE among the highest across all stations). The values of the mean and standard deviation over the 1980–2018 period for each dataset are presented in the legends of the figures.

In general, indices obtained with approximation A1 show similar temporal variations as the control data; the differences between the standard deviations are less than 1 day. The minima and maxima occur at the same time, although the approximation is subject to the small negative mean biases discussed earlier. However, this bias is reduced if one is interested in anomalies rather than absolute values (not shown).

For situations when models do not provide daily RHmin, we recommend applying a bias correction method against a target dataset with hourly data, thereby avoiding the need for direct approximation of HXmax by allowing the bias correction to perform the correction implicitly. One way to do this is to correct the approximated daily HXmax (obtained with RH daily mean values) using the index obtained from hourly values of the target dataset. Figure 9 presents an example for HXmax30 using the Quantile Delta Mapping bias correction method (Cannon *et al.*, 2015) on daily HXmax obtained from approximations A2 and A3, for the Montreal station. The target data used for correction is HXmax30 obtained from hourly HX. The values of the mean and standard deviation over the 1980–2018 period for each dataset are presented in the legends of the figures. Both approximations have very large biases for HXmax30: +11-day mean bias between the control dataset and approximation A3 and −21-day mean bias between the control dataset and approximation A2. Those are highly reduced (mean bias of 1 day or less) using the bias correction.

Another option for bias correction when daily RHmin is not available consists of using a multivariate bias correction that corrects the daily RHmean and daily Tmean/Tmax from the model, with the RH and T_a hourly values at the

time of HXmax provided by the hourly target dataset; daily HXmax would then be computed using the bias corrected values.

In such situations where daily RHmin is not available, a target dataset with good historical representation of daily HXmax is needed so that bias correction can implicitly correct the daily estimations from models. Thus, a thorough evaluation of the target dataset and costs and benefits of different bias correction methods would be necessary before implementing either of the above approaches. These methods are beyond the scope of this paper but are a potentially promising avenue of future work.

4 | CONCLUSIONS AND RECOMMENDATIONS

There is a demand for future projections of heat-stress indices, like Humidex (HX), that are based on the exceedance of thresholds used in meteorological heat warning systems. As operational systems rely on hourly data, which are usually not available in climate model archives, the objective of this study was to find a method that permits the reliable estimation of HX indices using more commonly available daily data.

The proposed method is based on the observation that, statistically, daily maximum HX (HXmax) coincides with the time of daily maximum air temperature (Tmax), which is also when relative humidity (RH) is at its daily minimum (RHmin). Therefore, daily HXmax can be approximated using daily Tmax and daily RHmin (approximation A1). Distributions of daily HXmax from this approximation are very similar to those calculated directly from hourly data for all stations used in the analysis. Using Tmax and RHmean (approximation A3), instead of Tmax and RHmin, adds positive errors as RHmean overestimates RH at the time of HXmax. The errors are even greater (and negative) if Tmean and RHmean are used (approximation A2) because Tmean underestimates temperature values at the time of HXmax and has a greater impact than RH on the HX. A more detailed analysis of approximations A2 and A3 is beyond the scope of the paper.

Results obtained for the threshold exceedance indices confirm the observations for daily HXmax. The approximated values with the approximation A1 present just a small negative bias (climatological mean biases of fewer than 2 days for most of the stations). Therefore, the proposed A1 approximation could be used for estimating threshold-based HX indices when daily Tmax and daily RHmin are available (e.g., Eyring *et al.*, 2016 for some CMIP6 models).

However, not all climate models include archived values of daily RHmin, which has led to the use of daily mean variables to compute HX indices (e.g., Scoccimarro *et al.*, 2017; Neethu and Ramesh, 2022). This short study demonstrates that threshold-based HX indices calculated using daily RHmean are highly underestimated when combined with daily Tmean and overestimated when combined with daily Tmax. A bias correction of the daily values against a target dataset with hourly values is recommended in this situation.

Approximation A1 proposed in this study assumes a strong relationship between the diurnal cycles of T_a and RH and is validated over Canada, a country where the population is not accustomed to facing long and frequent hot and humid periods. Several scientific papers have shown that the diurnal cycle of T_a and RH correlate well in other regions with a hotter and more humid climate such as Kuala Lumpur in West Malaysia (Aktas *et al.*, 2020) and Singapore (Acero *et al.*, 2020). Examples of diurnal cycles for short periods are also presented in Reddy *et al.* (2021) at a tropical coastal station in India, in Idris *et al.* (2019) at Aceh in Indonesia, and in Calvo *et al.* (2018) at locations in Spain. Those studies indicate that the new proposed approximation could also hold over other climatic regions and has potential for applications at global scale.

This study focussed on humidex indices. However, the issue of lack of availability of hourly datasets for climate projections stands for the other heat-stress indices (and many climate indices relevant to other impacts). Threshold-based heat indices in particular will be biased if daily mean values are used as input variables instead of hourly values, without direct adjustment or careful consideration of the implications of leaving the adjustment implicitly to bias correction methods. Some of the heat indices are defined using temperature and vapour pressure (e.g., NOAA heat index, apparent temperature, simplified wet-bulb globe temperature and universal thermal climate index) and they can be computed using T_a and RH. Figures presented in Aktas *et al.* (2020) show that the diurnal cycle of NOAA heat index and of apparent temperature index potentially correlate with the T_a and RH diurnal circle, and a similar approximation as for HX may be applicable as well. Likewise, wet-bulb temperature can be computed using T_a, RH, and pressure; however, pressure does not have a diurnal cycle. A detailed study is recommended over the region of interest before extending the approximation to other indices.

ACKNOWLEDGEMENTS

The authors wish to thank the Meteorological Service of Canada for developing and archiving the hourly station data used in this study. Special thanks to Elaine Barrow

and Jeremy Fyke from CCCS/ECCC for their valuable comments and suggestions.

ORCID

Emilia Diaconescu https://orcid.org/0000-0001-9682-9304

REFERENCES

Acero, J.A., Koh, E.J.K., Pignatta, G. and Norford, L.K. (2020) Clustering weather types for urban outdoor thermal comfort evaluation in a tropical area. *Theoretical and Applied Climatology*, 139, 659–675. https://doi.org/10.1007/s00704-019-02992-9.

Aktas, Y.D., Wang, K., Zhou, Y., Othman, M., Stocker, J., Jackson, M., Hood, C., Carruthers, D., Latif, M.T., D'Ayala, D. and Hunt, J. (2020) Outdoor thermal comfort and building energy use potential in different land-use areas in tropical cities: case of Kuala Lumpur. *Atmosphere*, 11(6), 652. https://doi.org/10.3390/atmos11060652.

Alfano, F.R.D.A., Palella, B.I. and Riccio, G. (2010) Thermal environment assessment reliability using temperature—humidity indices. *Industrial Health*, 49(1), 95–106. https://doi.org/10.2486/indhealth.MS1097.

Boberg, F., Berg, P., Thejll, P., Gutowski, W.J. and Christensen, J.H. (2010) Improved confidence in climate change projections of precipitation further evaluated using daily statistics from ENSEMBLES models. *Climate Dynamics*, 35, 1509–1520.

Bush, E. and Lemmen, D.S. (Eds.). (2019) *Canada's Changing Climate Report*. Ottawa, ON: Government of Canada, 444 pp. Available at: https://changingclimate.ca/CCCR2019/ [Accessed on 19th April 2022].

Buzan, J., Oleson, K. and Huber, M. (2015) Implementation and comparison of a suite of heat stress metrics within the Community Land Model version 4.5. *Geoscientific Model Development*, 8(2), 151–170. https://doi.org/10.5194/gmd-8-151-2015.

Calvo, A.I., Baumgardner, D., Castro, A., Fernández-González, D., Vega-Maray, A.M., Valencia-Barrera, R.M., Oduber, F., Blanco-Alegre, C. and Fraile, R. (2018) Daily behavior of urban fluorescing aerosol particles in northwest Spain. *Atmospheric Environment*, 184, 262–277. https://doi.org/10.1016/j.atmosenv.2018.04.027.

Cannon, A.J., Sobie, S.R. and Murdock, T.Q. (2015) Bias correction of GCM precipitation by quantile mapping: How well do methods preserve changes in quantiles and extremes? *Journal of Climate*, 28(17), 6938–6959. https://doi.org/10.1175/JCLI-D-14-00754.1.

Chavaillaz, Y., Roy, P., Partanen, A.-I., Silva, L., Bresson, E., Mengis, N., Chaumont, D. and Matthews, H.D. (2019) Exposure to excessive heat and impacts on labour productivity linked to cumulative CO_2 emissions. *Scientific Reports*, 9(9), 1–11.

Diaconescu, E.P., Mailhot, A., Brown, R. and Chaumont, D. (2018) Evaluation of CORDEX-Arctic daily precipitation and temperature based climate indices over Canadian Arctic land areas. *Climate Dynamics*, 50, 2061–2085.

Dunne, J.P., Stouffer, R.J. and John, J.G. (2013) Reductions in labour capacity from heat stress under climate warming. *Nature Climate Change*, 3(1), 563–566.

Eyring, V., Bony, S., Meehl, G.A., Senior, C.A., Stevens, B., Stouffer, R.J. and Taylor, K.E. (2016) Overview of the Coupled Model Intercomparison Project Phase 6 (CMIP6) experimental design and organization. *Geoscientific Model Development*, 9(1), 1937–1958. https://doi.org/10.5194/gmd-9-1937-2016.

Giannopoulou, K., Livada, I. and Santamouris, M. (2014) The influence of air temperature and humidity on human thermal comfort over the greater Athens area. *Sustainable Cities and Society*, 10, 184–194. https://doi.org/10.1016/j.scs.2013.09.004.

Golbabaei, F., Heidari, H. and Shamsipour, A. (2021) The assessment of thermal conditions using humidex in different weather conditions: a case in different climates of Iran. *Journal of Health Sciences & Surveillance System*, 9(2), 127–134. https://doi.org/10.30476/JHSSS.2021.89141.1158.

Idris, N., Maswati, M., Usmawanda, T.N. and Sari, A.M. (2019) Effect of temperature and humidity on the visibility of mirage on the runway of sultan Iskandar Muda Airport, Aceh, Indonesia. *Journal of Physics and Its Applications*, 2(1), 67–71. https://doi.org/10.14710/jpa.v2i1.6220.

Infusino, E., Caloiero, T., Fusto, F., Calderaro, G., Brutto, A. and Tagarelli, G. (2021) Characterization of the 2017 summer heat waves and their effects on the population of an area of southern Italy. *International Journal of Environmental Research and Public Health*, 18, 970. https://doi.org/10.3390/ijerph18030970.

IPCC. (2013) Summary for policymakers. In: Stocker, T.F., Qin, D., Plattner, G.-K., Tignor, M., Allen, S.K., Boschung, J., Nauels, A., Xia, Y., Bex, V. and Midgley, P.M. (Eds.) *Climate Change 2013: The Physical Science Basis. Contribution of Working Group I to the Fifth Assessment Report of the Intergovernmental Panel on Climate Change*. Cambridge and New York, NY: Cambridge University Press.

IPCC. (2021) Summary for policymakers. In: Masson-Delmotte, V., Zhai, P., Pirani, A., Connors, S.L., Péan, C., Berger, S., Caud, N., Chen, Y., Goldfarb, L., Gomis, M.I., Huang, M., Leitzell, K., Lonnoy, E., Matthews, J.B.R., Maycock, T.K., Waterfield, T., Yelekçi, O., Yu, R. and Zhou, B. (Eds.) *Climate Change 2021: The Physical Science Basis. Contribution of Working Group I to the Sixth Assessment Report of the Intergovernmental Panel on Climate Change*. Cambridge and New York, NY: Cambridge University Press, pp. 3–32. https://doi.org/10.1017/9781009157896.001.

Kabela, E.D. and Carbone, G.J. (2015) NARCCAP model skill and bias for the southeast United States. *American Journal of Climate Change*, 4, 94–114.

Kjellstrom, E., et al. (2010) Daily and monthly temperature and precipitation statistics as performance indicators for regional climate models. *Climate Research*, 44, 135–150.

Kjellstrom, T., Lemke, B. and Otto, M. (2013) Mapping occupational heat exposure and effects in South-East Asia: ongoing time trends 1980–2011 and future estimates to 2050. *Industrial Health*, 51(1), 56–67. https://doi.org/10.2486/indhealth.2012-0174.

Martínez-Austria, P.F. and Bandala, E.R. (2018) Heat waves: health effects, observed trends and climate change. In: Sallis, P. (Ed.) *Extreme Weather*. London: IntechOpen. https://doi.org/10.5772/intechopen.75559.

Masterton, J.M. and Richardson, F. (1979) *Humidex: A Method of Quantifying Human Discomfort due to Excessive Heat and Humidity*, Vol. 45. Canada: Environment Canada Atmospheric Environment.

Maxino, C.C., McAvaney, B.J., Pitman, A.J. and Perkins, S.E. (2008) Ranking the AR4 climate models over the Murray–Darling basin using simulated maximum temperature, minimum temperature and precipitation. *International Journal of Climatology*, 28, 1097–1112. https://doi.org/10.1002/joc.1612.

McMichael, A.J. and Lindgren, E. (2011) Climate change: present and future risks to health, and necessary responses. *Journal of Internal Medicine*, 270, 401–413.

Mekis, É., Vincent, L.A., Shephard, M.W. and Xuebin, Z. (2015) Observed trends in severe weather conditions based on humidex, wind chill, and heavy rainfall events in Canada for 1953–2012. *Atmosphere-Ocean*, 53, 383–397.

Mistry, M.N. (2020) A high spatiotemporal resolution global gridded dataset of historical human discomfort indices. *Atmosphere*, 11(8), 835.

Mora, C., Dousset, B., Caldwell, I.R., Powell, F.E., Geronimo, R.C., Bielecki, C.R., Counsell, C.W.W., Dietrich, B.S., Johnston, E.T., Louis, L.V., Lucas, M.P., McKenzie, M.M., Shea, A.G., Rseng, H., Giambelluca, T.W., Leon, L.R., Hawkins, E. and Trauernicht, C. (2017) Global risk of deadly heat. *Nature Climate Change*, 7, 501–506. https://doi.org/10.1038/nclimate3322.

Neethu, C. and Ramesh, K.V. (2022) High resolution spatiotemporal variability of heat wave impacts quantified by thermal comfort indices. *Theoretical and Applied Climatology*, 109, 1181–1198. https://doi.org/10.1007/s00704-022-03987-9.

Overland, J.E. and Wang, M. (2021) The 2020 Siberian heat wave. *International Journal of Climatology*, 41(1), E2341–E2346. https://doi.org/10.1002/joc.6850.

Perkins, S.E., Pitman, A.J., Holbrook, N.J. and McAneney, J. (2007) Evaluation of the AR4 climate model's simulated daily maximum temperature, minimum temperature, and precipitation over australia using probability density functions. *Journal of Climate*, 20(17), 4356–4376. https://doi.org/10.1175/JCLI4253.1.

Perkins, S.E., Pitman, A.J. and Sisson, S.A. (2009) Smaller projected increases in 20-year temperature returns over Australia in skill-selected climate models. *Geophysical Research Letters*, 36, L06710. https://doi.org/10.1029/2009GL037293.

Perkins, S.E., Irving, D.B., Brown, J.R., Power, S.B., Moise, A.F., Colman, R.A. and Smith, I. (2012) CMIP3 ensemble climate projections over the western tropical Pacific based on model skill. *Climate Research*, 51, 35–58. https://doi.org/10.3354/cr01046.

Perkins-Kirkpatrick, S.E. and Lewis, S.C. (2020) Increasing trends in regional heatwaves. *Nature Communications*, 11, 3357. https://doi.org/10.1038/s41467-020-16970.

Pitman, A.J. and Perkins, S.E. (2009) Global and regional comparison of daily 2-m and 1000-hPa maximum and minimum temperatures in three global reanalyses. *Journal of Climate*, 22, 4667–4681. https://doi.org/10.1175/2009JCLI2799.1.

Philip, S.Y., Kew, S.F., van Oldenborgh, G.J., Anslow, F.S., Seneviratne, S.I., Vautard, R., Coumou, D., Ebi, K.L., Arrighi, J., Singh, R., van Aalst, M., Marghidan, C.P., Wehner, M., Yang, W., Li, S., Schumacher, D.L., Hauser, M., Bonnet, R., Luu, L.N., Lehner, F., Gillett, N., Tradowsky, J., Vecchi, G.A., Rodell, C., Stull, R.B., Howard, R. and Otto, F.E.L. (2021) Rapid attribution analysis of the extraordinary heatwave on the Pacific Coast of the US and Canada June 2021. *Earth System Dynamics: Discussion*. https://doi.org/10.5194/esd-2021-90. Preprint.

Reddy, T.V.R., Mehta, S.K., Ananthavel, A., Ali, S. and Rao, D.N. (2021) Evolution of the planetary boundary layer and its simulation over a tropical coastal station Kattankulathur (12.83°N, 80.04°E). *Theoretical and Applied Climatology*, 146, 1043–1060. https://doi.org/10.1007/s00704-021-03770-2.

Rothfusz, L.P. (1990) *The heat index equation (or, more than you ever wanted to know about heat index)*. Forth Worth, TX: NWS S. Reg. Headquarters. Tech. Attachment, SR/SSD 90-23. Available at: https://www.weather.gov/media/ffc/ta_htindx.PDF [Accessed on 19th April 2022].

Schwingshackl, C., Sillmann, J., Vicedo-Cabrera, A.M., Sandstad, M. and Aunan, K. (2021) Heat stress indicators in CMIP6: estimating future trends and exceedances of impact-relevant thresholds. *Earth's Future*, 9(3), e2020EF001885. https://doi.org/10.1029/2020EF001885.

Scoccimarro, E., Fogli, P.G. and Gualdi, S. (2017) The role of humidity in determining scenarios of perceived temperature extremes in Europe. *Environmental Research Letters*, 12(11), 114029. https://doi.org/10.1088/1748-9326/aa8cdd.

Sobie, S.R., Zwiers, F.W. and Curry, C.L. (2021) Climate model projections for Canada: a comparison of CMIP5 and CMIP6. *Atmosphere-Ocean*, 59(4–5), 269–284. https://doi.org/10.1080/07055900.2021.2011103.

Staiger, H., Laschewski, G. and Grätz, A. (2012) The perceived temperature–a versatile index for the assessment of the human thermal environment. Part A: scientific basics. *International Journal of Biometeorology*, 56(1), 165–176. https://doi.org/10.1007/s00484-011-0409-6.

Steadman, R.G. (1979) The assessment of sultriness. Part I: A temperature-humidity index based on human physiology and clothing science. *Journal of Applied Meteorology and Climatology*, 18, 861–873. https://doi.org/10.1175/1520-0450(1979)018<0861:TAOSPI>2.0.CO;2.

Středová, H., Středa, T. and Litschmann, T. (2015) Smart tools of urban climate evaluation for smart spatial planning. *Moravian Geographical Reports*, 23, 47–57. https://doi.org/10.1515/mgr-2015-0017.

Zhao, Y., Ducharne, A., Sultan, B., Braconnot, P. and Vautard, R. (2015) Estimating heat stress from climate-based indicators: present-day biases and future spreads in the CMIP5 global climate model ensemble. *Environmental Research Letters*, 10, 084013. https://doi.org/10.1088/1748-9326/10/8/084013.

How to cite this article: Diaconescu, E., Sankare, H., Chow, K., Murdock, T. Q., & Cannon, A. J. (2023). A short note on the use of daily climate data to calculate Humidex heat-stress indices. *International Journal of Climatology*, *43*(2), 837–849. https://doi.org/10.1002/joc.7833